Supplemental Material: Membrane-Mediated Dimerization of Spherocylindrical Nanoparticles

Abash Sharma[a], Yu Zhu[a], Eric J. Spangler[a], Jan-Michael Y. Carrillo[b], and Mohamed Laradji[a]

[a] *Department of Physics and Materials Science, The University of Memphis, Memphis, TN 38152, USA*

[b] *Center for Nanophase Materials Sciences, Oak Ridge National Laboratory, Oak Ridge, TN 37831, USA*

SI. SOFT POTENTIAL

In Eq. (1) of the main text, $U_0^{\alpha\beta}$ is a soft two-body potential, between beads of types α and β and is given by

$$U_0^{\alpha\beta}(r) = \begin{cases} \left(U_{\rm max}^{\alpha\beta} - U_{\rm min}^{\alpha\beta}\right) \frac{(r_m - r)^2}{r_m^2} + U_{\rm min}^{\alpha\beta} & \text{if } r \le r_m, \\ -2\, U_{\rm min}^{\alpha\beta} \frac{(r_c - r)^3}{(r_c - r_m)^3} + 3\, U_{\rm min}^{\alpha\beta} \frac{(r_c - r)^2}{(r_c - r_m)^2} & \text{if } r_m < r \le r_c, \\ 0 & \text{if } r > r_c, \end{cases} \tag{A1}$$

where $U_{\rm max}^{\alpha\beta} > 0$ and $U_{\rm min}^{\alpha\beta} \le 0$ for any pair (α, β). $U_{\rm min}^{\alpha\beta} = 0$ implies a fully repulsive interaction between α and β, and $U_{\rm min}^{\alpha\beta} < 0$ implies a short-range attraction between the two beads. The self-assembly of the lipids into thermodynamically stable bilayers is ensured by choosing $U_{\rm min}^{hh} = U_{\rm min}^{ht} = 0$ and strong enough negative value of $U_{\rm min}^{tt}$ [1].

SII. CONSTRUCTION OF A SPHEROCYLINDRICAL NANOPARTICLE

A spherocylindrical nanoparticle (SCNP) is constructed using the approach shown in Fig S1. At first, a geodesic polyhedron is created as a good approximation to a sphere starting from an icosahedron. An icosahedral grid, which circumscribes a sphere of radius 10 units, was triangulated three times resulting in 642 vertices and 1280 elementary triangles. The coordinates of these beads were ultimately projected onto the circumscribed sphere making sure that all the vertices lie on the sphere and are at a distance of 10 units from its center, as shown by Fig S1(a). The final vertices all have 6 nearest neighbors, except for 12 initial icosahedron vertices which have 5 nearest neighbors. The average distance between the nodes is 1.5 units.

The sphere is then split symmetrically through the plane ($x = 0$) into left and right hemispheres, which will form the two ends of the SCNP (Fig S1(b)), such that the NPs principal axis is along the x-axis. The points that lie on the yz-plane (great circle) is shared by both hemispheres. The right hemisphere is then translated by a distance $\Delta x\ l$ to the right, which is determined from the desired aspect ratio, α, of the NP. For instance, to generate a NP of $\alpha = 1.6$, $\Delta x = 1.6 \times 20 - 20 = 12$ Hence, all vertices on the right hemisphere are translated by 12 units towards the right

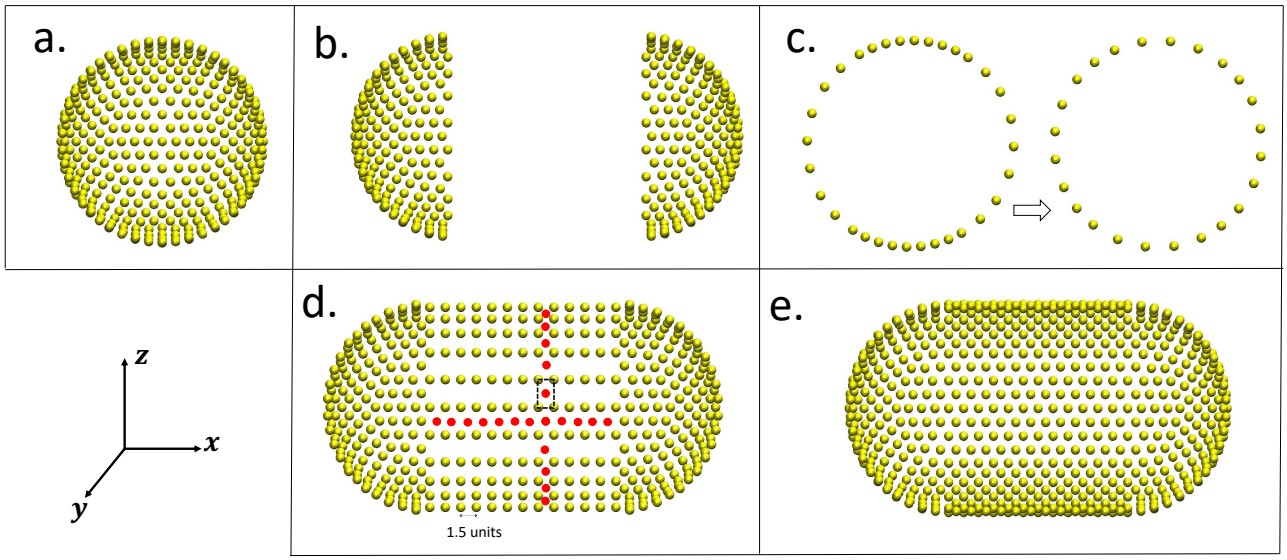

FIG. S1. Steps showing the construction of a spherocylindrical NP. (a) Original tessellated sphere with 642 vertices. (b) Two hemispherical caps of the NP are constructed by splitting the original sphere. (c) Rearrangement of the vertices on the great circle such that the vertices are equidistant. (d) Generation of the vertices of the cylindrical portion of the NP. (e) Final tessellated NP.

along the x-axis. It is important to note that the points on the circumference of the great circle are not equidistant from each other, as demonstrated by the left configuration in Fig. S1(c). To mitigate this problem, the points on the great circle are rearranged such that they are at a uniform distance from each other (Fig S1(c)).

The next step generate the vertices on the surface of cylindrical part of the NP. First, replicas of the great circle are constructed between the left and right great circles, and are separated by a distance of 1.5 units. The number of these replicas depends on α. Vertices are then added at the center of each quadrilateral formed by four nearest neighbors (e.g. dashed quadrilateral in Fig S1(d)). We note that this approach leads to some defects in the regions where the cylindrical surface is connected to the two hemispheres. These defects are formed because of the rearrangement of the points on the circumference of the great circles of the hemispheres. In particular, there are vertices in these regions with only 4 nearest neighbors. These points are connected to their neighbors with some bonds that are longer than 2 units. This problem is solved by identifying the defect regions, and inserting vertices in the middle of the defect region. Finally, we project all the points on the surface of hemispheres at a distance of 10 units from their respective centers and project the points on the surface of the cylindrical part on a cylinder with radius 10 units from the cylindrical axis. The final constructed SCNP is shown in Fig S1(e). The NP is then scaled conformally to the desired radius.

SIII. ENERGY DENSITY CALCULATION

The adhesion energy density is defined as $\xi = |U_{adh}|/A_{adh}$, where U_{adh} is the net potential energy between the NP and the membrane and A_{adh} is the area of the NP adhering to the membrane. To determine the adhesion energy density, simulations of a spherical NP of diameter D adhering to a tensionless planar bilayer are performed at different

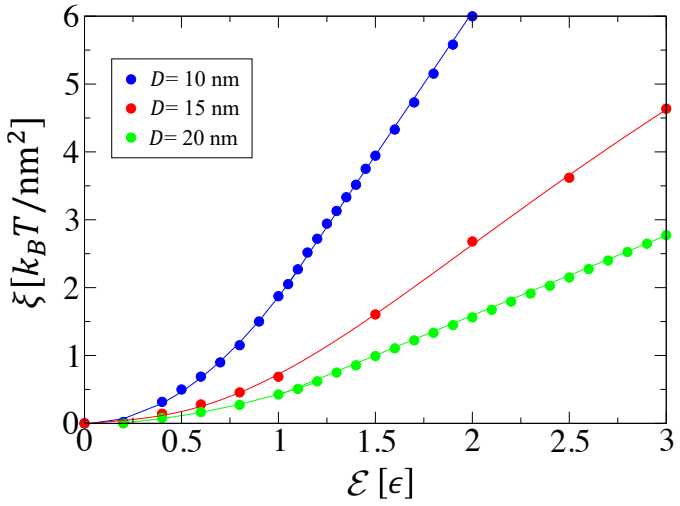

FIG. S2. The adhesion energy density, ξ, versus the interaction strength, $\mathcal{E}$, between a NP n-bead and a lipid h-bead, for different values of the NP's diameter.

values of $\mathcal{E}$. Here, an n bead adheres to the membrane if it interacts with at least one h bead of the membrane, i.e. if its distance from the h bead is less than r_c. Fig. S2 depicts the adhesion energy density versus distance $\mathcal{E}$ for NPs with diameter $D = 10$, 15 and 20 nm. This figure shows that ξ dependence on $\mathcal{E}$ is not linear for low values of $\mathcal{E}$, but becomes linear as $\mathcal{E}$ further increases. This figure also shows that for a given $\mathcal{E}$, ξ decreases with D. This is simply due to the fact that the number of beads on a spherical NP is fixed (642 beads), regardless of its size.

SIV. DISTANCE VS TIME AT $\xi = 0.69\, k_BT/\text{nm}^2$

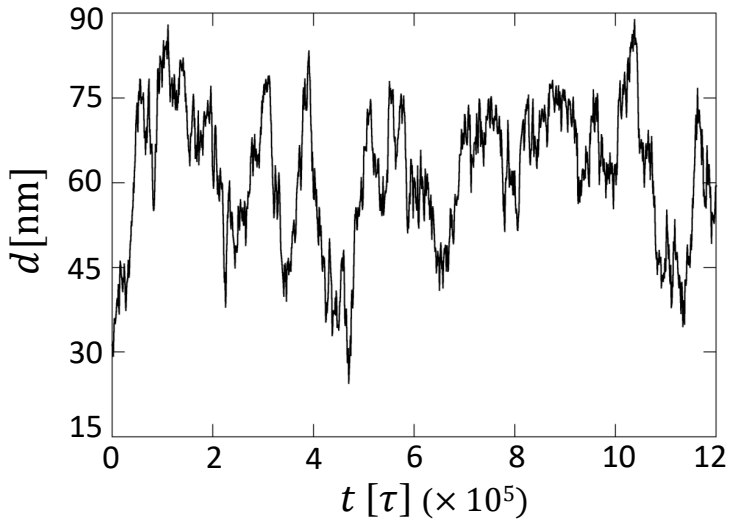

FIG. S3. Distance between the centers of mass of two SCNPs, with $D = 10$ nm and $\rho = 1.75$, vs time at $\xi = 0.69\, k_BT/\text{nm}^2$. This figure shows that the SCNPs are highly diffusive and that at times, the SCNPS encounter each other.

SV. INITIAL CONFIGURATION

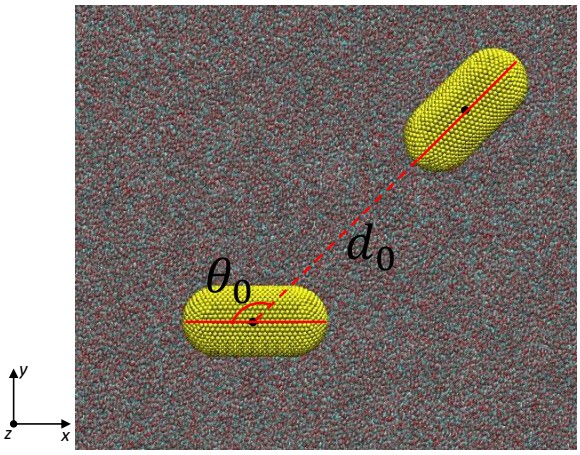

FIG. S4. An initial configuration of two SCNPs showing the initial angle θ_0 between their principal axes and the distance d_0 between their centers of mass. The membrane is parallel to the xy-plane.

SVI. EFFECT OF INITIAL DISTANCE AT $\xi = 1.83\, k_BT/\text{nm}^2$

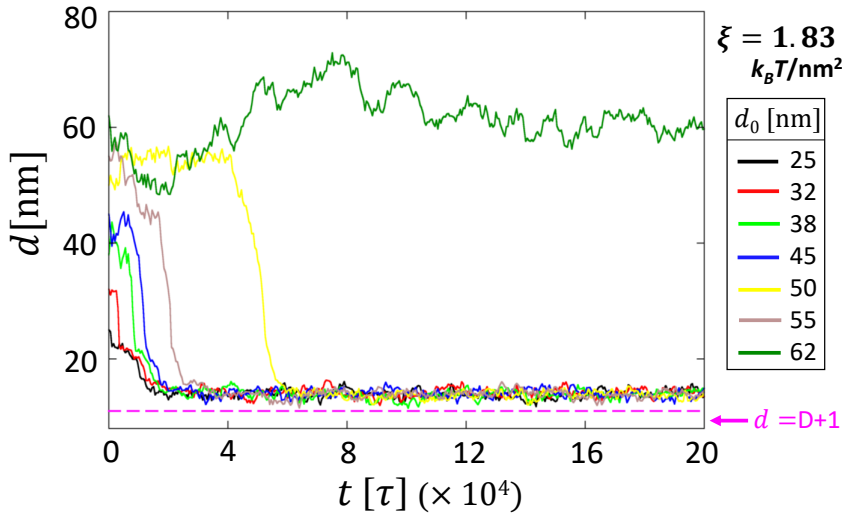

FIG. S5. Distance between the centers of mass of two SCNPs, with $D = 10$ nm and $\rho = 2.13$, vs time for different values of d_0 at $\xi = 1.83\, k_BT/\text{nm}^2$. The initial seed in these simulations are different from those in Fig. 3(C). This figure demonstrates that the results are independent of initial randomness.

SVII. KINETIC PATHWAY TO THE NORMAL MONOMERIC ADHESION MODE

Fig. S6 shows the kinetics following adhesion of two SCNPs with $D = 10$ nm and $\rho = 2.13$ at $\xi = 1.83\, k_BT/\text{nm}^2$ and at an initial distance between them $d_0 = 50$ nm and initial angle $\theta_0 = 45°$. Due to the fact that d_0 here is relatively large, the SCNPs do not dimerize. Instead, they individually rotate at $t \approx 4 \times 10^4$ to the normal monomeric mode.

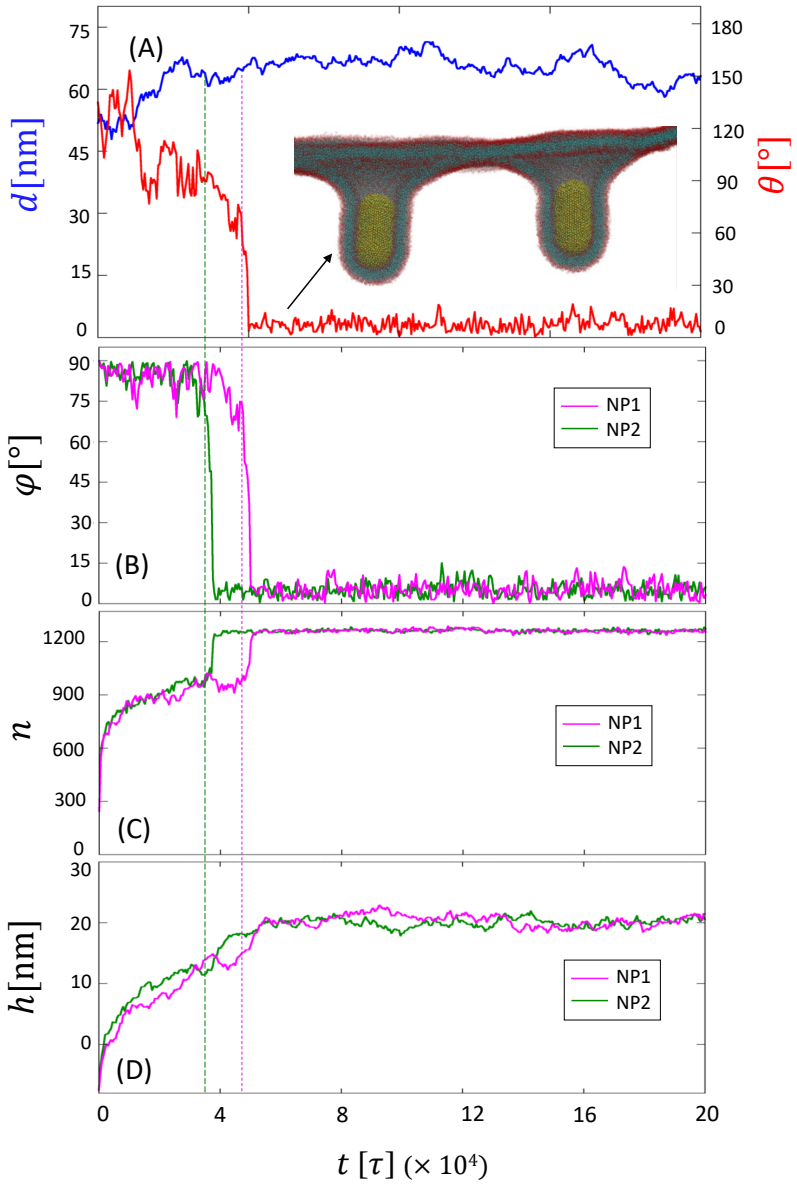

FIG. S6. Kinetic pathway to the normal monomeric mode in the case where two SCNPs, with $D = 10$ nm and $\rho = 2.13$ at $\xi = 1.83\, k_BT/\text{nm}^2$, initially at a distance $d_0 = 50$ nm and angle $\theta_0 = 45°$. (A) Distance d between the SCNPs vs time (left y-axis) and angle θ vs time (right y-axis). Also shown in (A) is the side-view snapshot of the equilibrated system. (B) Angles between the SCNPs and the z-axis. (C) Numbers of lipid head beads in contact with the SCNPs. (D) Depths of the SCNPs, along the z-axis, with respect to the average height of the membrane.

SVIII. CURVATURE ENERGY CALCULATION

In order to calculate the curvature energy, we use a local Monge representation of the Helfrich Hamiltonian [2]. This approach is valid since the Helfrich Hamiltonian is invariant under arbitrary rotation. The calculation proceeds through the following steps (See Fig. S7):

1) For each lipid i, all neighboring lipids within the same leaflet and within a range $\lambda = 0.865\, r_m$ are identified, and their average normalized end-to-end vector, $\hat{\mathbf{n}}_i$, is calculated.

2) A unit vector, tangent to the membrane at lipid i, $\hat{\mathbf{t}}_i = \hat{\mathbf{n}}_i \times \hat{\mathbf{z}}$, is determined.

3) The portion of the membrane, composed of all lipids within the distance $3\sqrt{2}\lambda$ from lipid i and belonging to the same leaflet, is then rotated around the tangent vector $\hat{\mathbf{t}}_i$ by the angle $\theta = \cos^{-1}(\hat{\mathbf{z}} \cdot \hat{\mathbf{n}}_i)$, using the following matrix [4]

$$\mathbf{R} = \begin{bmatrix} t_{i,x}^2(1-c)+c & t_{i,x}t_{i,y}(1-c)-t_{i,z}s & t_{i,x}t_{i,z}(1-c)+t_{i,y}s \\ t_{i,x}t_{i,y}(1-c)+t_{i,z}s & t_{i,y}^2(1-c)+c & t_{i,y}t_{i,z}(1-c)-t_{i,x}s \\ t_{i,x}t_{i,z}(1-c)-t_{i,y}s & t_{i,y}t_{i,z}(1-c)+t_{i,x}s & t_{i,z}^2(1-c)+c \end{bmatrix} \tag{A2}$$

where $t_{i,x}$, $t_{i,y}$ and $t_{i,z}$ are the three components of the unit tangent vector $\hat{\mathbf{t}}_i$. $c = \cos\theta$ and $s = \sin\theta$. The transformed z-axis (labeled $\tilde{z}$ is now locally normal to the region of the membrane around lipid i.

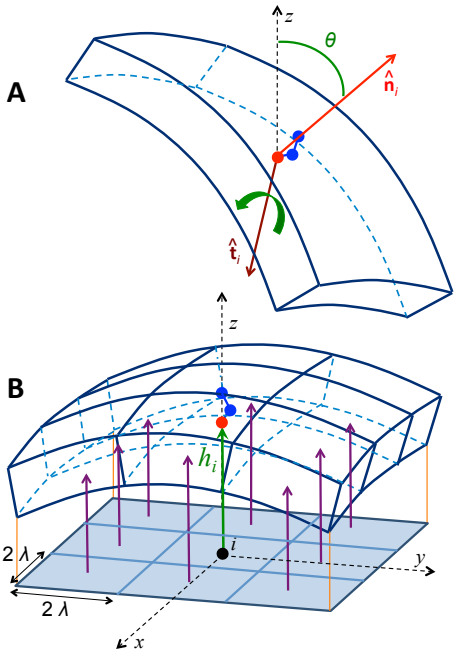

FIG. S7. A schematic representation of a portion of the lipid bilayer, centered at lipid i before rotation (A) and after rotation (B). In (A), $\hat{\mathbf{n}}_i$ is a unit vector in the direction of the mean of the end-to-end vectors of lipids in a small region around i as explained in the text. $\hat{\mathbf{t}}_i = \hat{\mathbf{n}}_i \times \hat{\mathbf{z}}$ is a local tangent vector that is normal to both the z-axis and $\mathbf{n}_i$. The bilayer is rotated around the vector $\mathbf{t}_i$ by the angle θ between $\hat{\mathbf{n}}_i$ and the z-axis. Note that the bilayer is not descritized before rotation. The discretised xy-plane in (B) is parallel to the tangent plan to the membrane at i. The vertical purple arrows indicate the heights of the descritized parts of the leaflet, containing lipid i. From Spangler *et al.* [3].

4) The tangent plane to the rotated portion of the membrane leaflet around lipid i is then discretized into small squares of area $a_p = (2\lambda)^2$, such that the projection of the head bead of lipid i is at the center of its projection square, as shown by Fig. 6 in Ref. [3].

5) The local heights of the leaflet in the neighborhood of i are then determined, which allow for the calculation of the first order partial derivatives $h_{i,\tilde{x}}$, $h_{i,\tilde{y}}$, and second order partial derivatives $h_{i,\tilde{x}\tilde{x}}$, $h_{i,\tilde{x}\tilde{y}}$ and $h_{i,\tilde{y}\tilde{y}}$ using the finite difference method based on both nearest and next-nearest neighbors.

6) The local extrinsic curvature of the leaflet at lipid i is then calculated using the following approximation,

$$K_i = \frac{\left(1 + h_{i,\tilde{y}}^2\right) h_{i,\tilde{x}\tilde{x}} + \left(1 + h_{i,\tilde{x}}^2\right) h_{i,\tilde{y}\tilde{y}} - 2h_{i,\tilde{x}} h_{i,\tilde{y}} h_{i,\tilde{x}\tilde{y}}}{\left(1 + h_{i,\tilde{x}}^2 + h_{i,\tilde{y}}^2\right)^{3/2}}. \tag{A3}$$

7) The curvature energy of the bilayer is then calculated as

$$F_{\text{curv}} = \sum_{i=1}^{N_{\text{lip}}} \Delta\mathcal{A}_i \frac{\kappa}{4} K_i^2, \tag{A4}$$

where 4 in the denominator accounts for the fact that the curvature energy is calculated for each leaflet separately, and κ being the bending modulus of the bilayer. $\Delta\mathcal{A}_i$ in the equation above is the local area of the leaflet at lipid i, and is given by

$$\Delta\mathcal{A}_i = (a_p/n_i)\left(1 + h_{i,\tilde{x}}^2 + h_{i,\tilde{y}}^2\right)^{1/2}, \tag{A5}$$

where n_i is the number of lipids whose projection fall onto the local square centered at i in the locally rotated coordinate system.

We emphasize that this approach does not account for the entropic contributions to the free energy of the lipid membrane [3]. Therefore, F_{curv} is an approximation of the curvature free energy.

[1] M. Laradji, P. B. Sunil Kumar, and E. J. Spangler, *Journal of Physics D: Applied Physics*, **49**, 293001 (2016).

[2] W. Helfrich, Z. Naturforsch. C: J. Biosci. **28**, 693 (1973).

[3] E. J. Spangler, P. B. Sunil Kumar, and M. Laradji, Soft Matter **14**, 5019 (2018).

[4] P. D. Lin, *Advanced Geometrical Optics* (Springer, 2017).